Circuit reorganization in the *Drosophila* mushroom body calyx accompanies memory consolidation

Lothar Baltruschat[1¶], Philipp Ranft[1¶], Luigi Prisco[1¶], J. Scott Lauritzen[2], André Fiala[3], Davi D. Bock[2,4] and Gaia Tavosanis[1,5*]

[1]Center for Neurodegenerative Diseases (DZNE), Bonn, Germany

[2]Janelia Research Campus, Howard Hughes Medical Institute, Ashburn, United States

[3]Molecular Neurobiology of Behaviour, University of Göttingen, Germany

[4] Department of Neurological Sciences, University of Vermont, Burlington, VT, USA

[5]LIMES Institute, University of Bonn, Germany

¶Equal contribution

**To whom correspondence should be addressed*

Short title: Structural and functional plasticity in the adult mushroom body

Keywords: Drosophila, structural plasticity, functional plasticity, memory consolidation, mushroom body, microglomerulus.

Summary

The capacity of utilizing past experience to guide future action is a fundamental and conserved function of the nervous system. Associative memory formation initiated by the coincident detection of a conditioned stimulus (CS, e.g. odour) and an unconditioned stimulus (US, e.g. sugar reward) can lead to a short-lived memory trace (STM) within distinct circuits [1-5]. Memories can be consolidated into long-term memories (LTM) through processes that are not fully understood, but depend on *de-novo* protein synthesis [6, 7], require structural modifications within the involved neuronal circuits and might lead to the recruitment of additional ones [8-17]. Compared to modulation of existing connections, the reorganization of circuits affords the unique possibility of sampling for potential new partners [18-20]. Nonetheless, only few examples of rewiring associated with learning have been established thus far [14, 21-24]. Here, we report that memory consolidation is associated with the structural and functional reorganization of an identified circuit in the adult fly brain. The formation and retrieval of olfactory associative memories in *Drosophila* requires the mushroom body (MB) [25]. We identified the individual synapses of olfactory projection neurons (PNs) that deliver a conditioned odour to the MB and reconstructed the complexity of the microcircuit they form. Combining behavioural experiments with high-resolution microscopy and functional imaging, we demonstrated that the consolidation of appetitive olfactory memories closely correlates with an increase in the number of synaptic complexes formed by the PNs that deliver the conditioned stimulus and their postsynaptic partners. These structural changes result in additional functional synaptic connections.

42 **Results**

43 To start addressing systematically the mechanisms that support memory
44 consolidation, we sought to investigate the properties of identifiable synapses in the
45 MB of the adult brain of *Drosophila* after the establishment of LTM. Within the main
46 MB input compartment, the calyx (MBC), PNs deliver olfactory information through
47 cholinergic synapses to the intrinsic MB neurons, the Kenyon cells (KCs) (Figure 1A).
48 In the MBC, large olfactory PN boutons are enwrapped by the claw-like dendrite
49 termini of ~11 KCs on average [26, 27], thereby forming characteristic synaptic
50 complexes, the microglomeruli (MGs) [28] (Figure 1A-E), which display functional and
51 structural plasticity in adaptation and upon silencing [29-31]. The pheromone and
52 odorant 11-cis-Vaccenylacetate (cVA) activates specifically those PNs that project
53 their dendrites to the DA1 glomerulus in the antennal lobe (AL) [32-34] (Figure 1A, B;
54 DA1-PNs). The DA1 glomerulus is mostly excluded from complex processing of
55 sensory information in the AL [35, 36], suggesting that by genetically marking the
56 DA1 PNs we could identify the individual boutons in the MBC that deliver the
57 olfactory response to cVA. We tested this by recording with volumetric calcium
58 imaging the response to odour stimulation in the MBC of animals expressing a
59 genetically encoded calcium indicator tethered at the KC postsynapses (*MB247-*
60 *homer::GCaMP3*) [30] in combination with a presynaptic fluorescent tag (*UAS-td-*
61 *Tomato*) expressed in DA1-PNs only (Figure 1C). Regions of interest (ROIs)
62 containing fluorescently labelled DA1-MGs showed a postsynaptic response
63 specifically tuned to cVA stimulation (84% of the fluorescently labelled MGs
64 responded to cVA only; n=7 animals, 72 boutons; Figure 1C).

65 Taken together, by selecting the combination of the cVA odorant and the DA1 subset
66 of PNs we established fly lines in which we can track a fly's neuronal response
67 towards a specific odour on the level of individual synaptic complexes in the MBC
68 (Figure 1A-C).

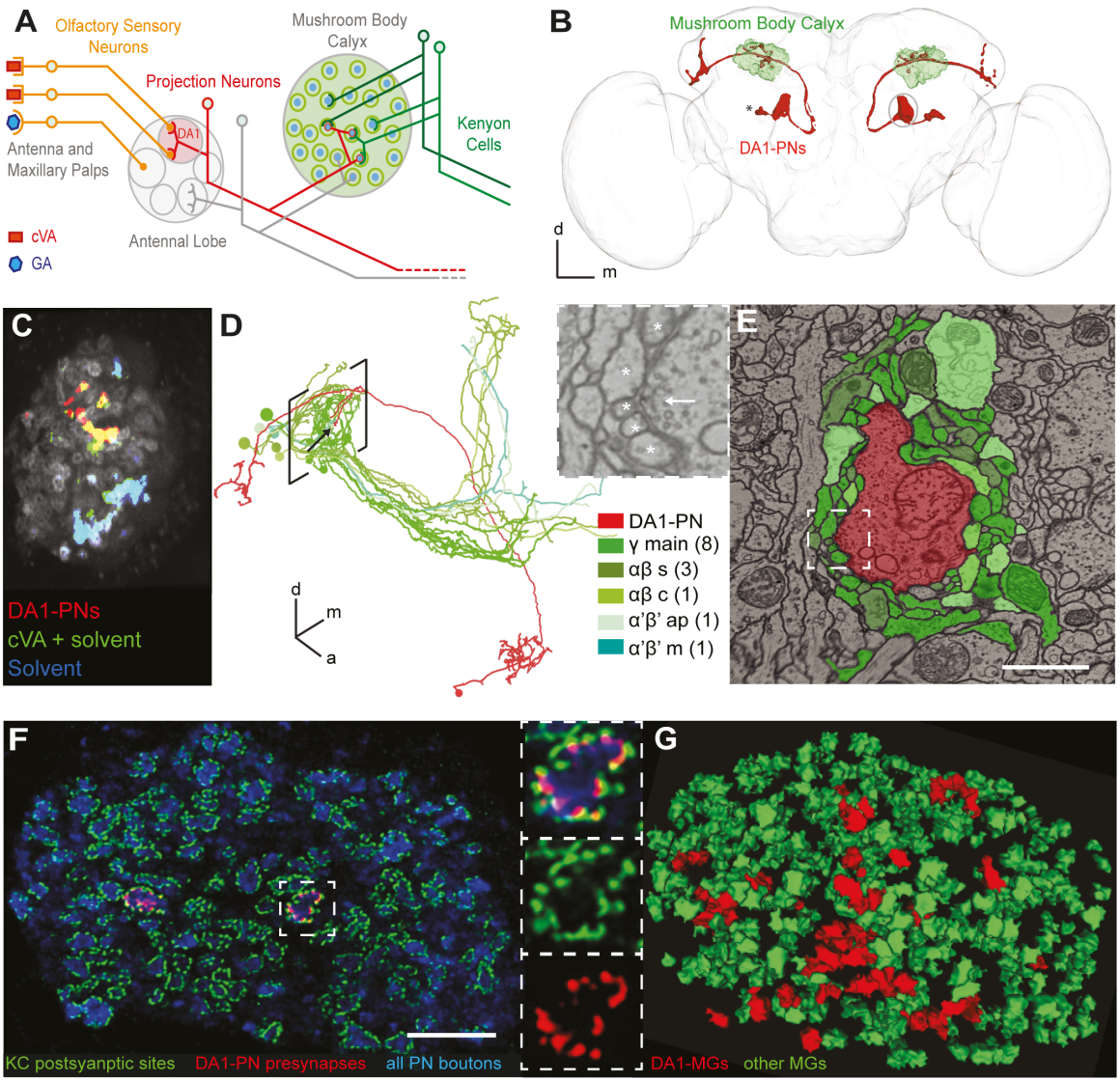

69

70 **Figure 1 | Identification of the synapses in the MBC responding to cVA odour**
71 **stimulation**

72 **(A)** Schematic representation of the olfactory circuit starting from the activation of specific
73 Olfactory Sensory Neurons (OSNs) by two exemplary odours cVA and GA. In the AL cVA-
74 responsive OSNs converge to the DA1 glomerulus (pale red), where they synapse onto DA1-
75 PNs (red). These deliver the cVA signal to the MBC via axon collaterals that terminate with
76 boutons forming large synaptic complexes, the MGs. Postsynaptic KCs are represented in
77 green. **(B)** Reconstruction from a full confocal serial section set of the DA1-PNs (red;

78 *R37H08-Gal4> UAS GAP43::Venus*); MBC (green; *MB247-Dα7::GFP*); DA1-PN cell bodies
79 (*); brain neuropil (light grey; α-synapsin antibody). **(C)** Volumetric calcium imaging of the
80 calyx of flies carrying *MB247-Homer::GCaMP3* (grey) and in which DA1-PNs are genetically
81 labelled (red; *R37H08-Gal4> UAS tdTomato*). cVA-elicited postsynaptic responses (green)
82 are specific to DA1-PNs, confirmed by the overlap between the two channels (yellow).
83 Generic response to the solvent (cyan= overlap of the responses to cVA+ EtOH, green, and
84 to EtOH only, blue). **(D)** Single DA1-PN (red) and the 14 KCs (green) postsynaptic to the
85 DA1-PN bouton indicated by the arrow. Tracings performed on the EM FAFB dataset [37].
86 Square brackets indicate location of MBC. Different green shades represent different KC
87 subtypes (as in E). Numbers in brackets in the legend represent the number of cells. **(E)**
88 Single EM section through the MG (arrow in D); scale bar = 1 µm. White square is magnified
89 in left top panel with arrow pointing to a T-bar of the AZ and * labelling fine dendritic
90 postsynaptic profiles of KCs. **(F)** Single plane confocal image of the MBC displaying PN
91 boutons (blue; α-synapsin antibodies); the PSDs of KCs (green; *MB247-Dα7::GFP*) and the
92 AZs of DA1-PN boutons only (red; *R37H08-Gal4 > UAS-brp-short*^{cherry}) identifying the cVA-
93 responsive MGs. Scale bar = 10 µm. The MG in the white square is magnified in the right
94 panels. **(G)** Automated 3D reconstruction of a confocal stack, including the image shown in
95 (F). The reconstruction of MGs is based on Dα7-GFP (green) (see also Figure S1) and MGs
96 receiving presynaptic input from DA1-PNs are marked by Brp–short^{cherry} (red). All other MGs
97 are in green. Full genotypes used and statistics for all Figures are included in the
98 Supplemental Genotypes and Statistics table.

99

100 To gain insight into the complexity of the MG microcircuit formed by a single DA1-PN
101 bouton we took advantage of the availability of a whole brain electron microscopy
102 (EM) volume of an adult female fly (FAFB) [37]. In this set of data we reconstructed a
103 complete MG connectome by tracing neurites from every pre- and postsynaptic
104 contact of a DA1-PN bouton until the corresponding neuron's identity was
105 anatomically determinable (Figure 1D, E; Supplementary Table 1). This particular
106 DA1-PN bouton made 33 excitatory, cholinergic contacts, all polyadic and identifiable
107 by the presence of a T-bar and of a synaptic cleft (Figure 1E, inset), apposed to 277
108 postsynaptic profiles. Most profiles (248) postsynaptic to the bouton originated from
109 14 KCs of 5 different subtypes: γmain (8), αβs (3), αβc (1), α'β'ap (1) and α'β'm (1)
110 [38](Figure 1D, E; Supplementary Table 1, Movie 1). γmain profiles were thus the
111 most abundant in this particular bouton, although DA1-PN boutons are located within
112 a region of the MBC predominantly occupied by αβs KCs [39]. Each KC contacted
113 the bouton with a single claw receiving 8 to 25 presynaptic inputs from the PN

114 bouton, in line with previous estimates [26, 31]. Within the MG, the bouton received
115 presynaptic input from 4 cells: two additional γmain KCs forming divergent triads that
116 included a KC, the PN bouton and the anterior paired lateral neuron (APL) [40]; APL
117 itself and one of the two Mushroom Body Calyx 1 neurons (MB-C1) (Supplementary
118 Table 1 and described elsewhere). Taken together, a single MG represents a highly
119 complex microcircuit, involving many neurons (19 in this example) of different types
120 (here 8).

121 To investigate whether such a complex structure could undergo plastic changes, we
122 designed a setup to reveal and measure the properties of identifiable MGs following
123 olfactory conditioning.

124 In confocal images, we highlighted cVA responsive MGs in the MBC by expressing
125 only in DA1-PNs the presynaptic active zone (AZ) marker Brp-short^{cherry} (Figure 1F)
126 [29, 41]. The postsynaptic densities (PSDs) of KC dendrites were decorated by cell-
127 type specific genetic expression of a GFP-tagged Dα7 subunit of the acetylcholine
128 receptor (Figure 1F) [29]. MGs could thus be identified with a software-based
129 automated 3D-reconstruction tool exploiting the *MB247-Dα7::GFP* signal and were
130 then classified as DA1-PN positive if they additionally displayed Brp-short^{cherry} co-
131 labelling (DA1-MG; Figure 1G; Figure S1). Further, we established an appetitive
132 associative conditioning paradigm using cVA or geranyl acetate (GA) as CS in STM
133 or LTM paradigms (Figure 2A; Figure S2A-C; see Methods) and applied it to flies
134 expressing the reporters mentioned above (Figure 2B, F, J). Alternatively, we mock-
135 trained the flies by presenting each odour or the sugar reward at 2 min intervals to
136 avoid the formation of appetitive association (Figure 2A, B, F, J) [42]. GA was chosen
137 as it activates a separate and non-overlapping set of PNs in comparison to cVA [43]

138 and 5% EtOH was added to provide a food-related context to the starved flies (Figure
139 S2B) [36, 44]. To assess if MGs formed by DA1-PN boutons (DA1-MGs) underwent
140 morphological modifications after learning, we prepared for confocal imaging female
141 fly brains dissected at 1 min (STM) or at 24 h (LTM) after training. After STM
142 establishment (Figure 2B) the total number, MG volume and lumen volume of DA1-
143 MGs was unchanged in cVA conditioned (cVA CS+) flies compared to the GA
144 conditioned (GA CS+) or mock control groups (average MG numbers: mock 28.91;
145 GA CS+ 30.40; cVA CS+ 28.76; n= 10-17; Figure 2C-E). However, in the LTM
146 paradigm (Figure 2F) the MG volume and the lumen volume of DA1-PN MGs were
147 decreased in cVA CS+ flies compared to GA CS+ or to mock-control flies (Figure 2G,
148 H). In addition, the total number of DA1-MGs was increased (average MG numbers:
149 mock 27.31; GA CS+ 27.47; cVA CS+ 32.06; n= 18-32; Figure 2I). Thus, LTM, but
150 not STM, was accompanied by an input-specific structural reorganization of the MBC
151 circuit, including an increase in MGs number. These changes were specific to the
152 conditioned odour, as they did not appear in the DA1-MGs when the conditioned
153 odour was GA. These data suggest that the neurons delivering the CS form new
154 boutons, which are of smaller size and enveloped by KC claws.

155 Olfactory associative learning relies on the function of the Ca^{2+}/CaM-dependent
156 adenylyl cyclase Rutabaga [42, 45, 46] and a defining trait of LTM is its dependence
157 on protein synthesis [6, 47, 48]. Indeed, a mutation in the *rutabaga* gene (*rut*^{2080}) [49]
158 or feeding flies with the protein synthesis inhibitor cycloheximide (CHX) immediately
159 after training abolished LTM (Figure 2J; Figure S2D). Importantly, loss of *rut* function
160 or CHX feeding also suppressed the structural changes in the DA1-MGs supporting
161 the correlation between LTM formation and structural changes in the circuit (Figure
162 2K-M; Figure S2E-G).

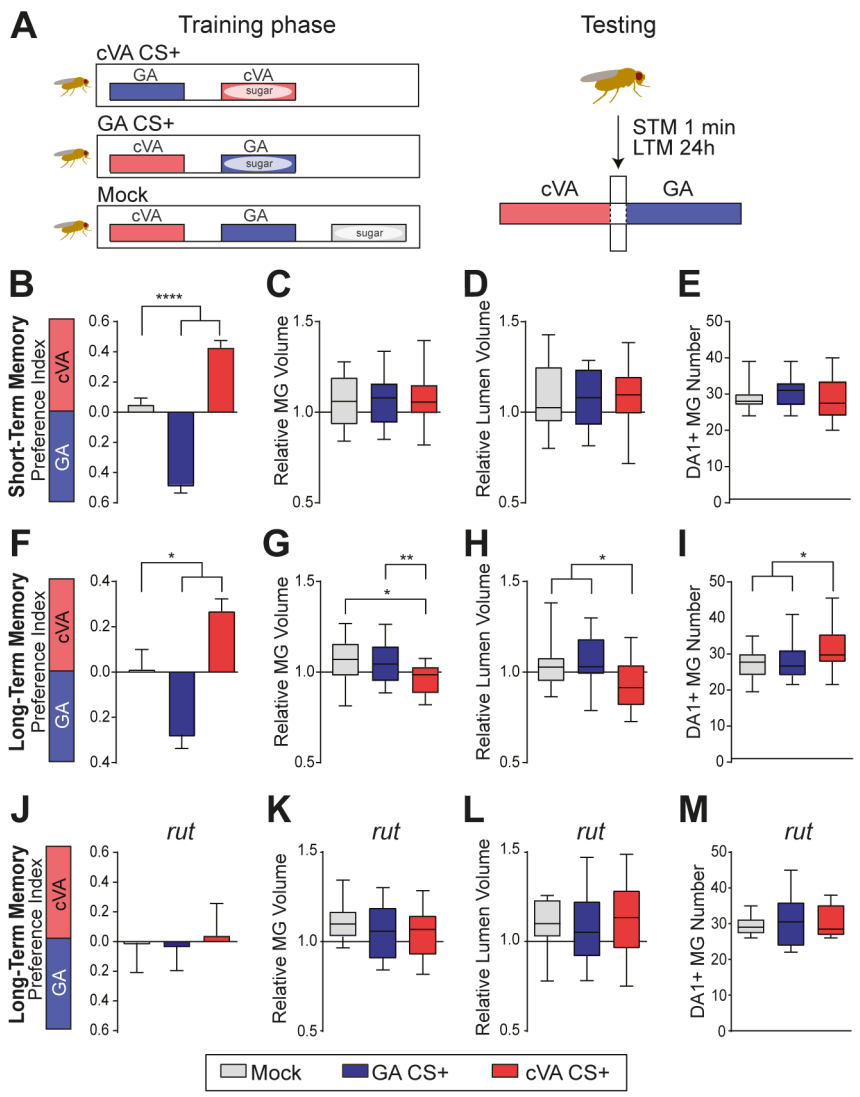

Figure 2 | Microglomeruli undergo structural changes upon appetitive long-term memory formation

(A) Schematic illustration of the appetitive conditioning paradigm. For training, the conditioned odour cVA (red box) or GA (blue box) is paired with sugar. In STM experiments flies are trained for 2 min with a 2 min interval between CS+ and CS- presentation and tested 1 min after training. In LTM experiments flies are trained for 5 min + 5 min with a 2 min stimulus interval and are tested 24 h after training. In the mock control the two odours and the sugar reward are presented in a temporally spaced sequence with a 2 min inter-stimulus pause. **(B, F, J)** Preference indices of flies *R37H08-Gal4/MB247-Dα7::GFP, UAS-brp-short*^{cherry} in the STM (n = 19 – 25) **(B)** or in the LTM (n = 14 - 19) paradigm **(F)** and preference index of *rut* mutant flies in LTM **(J)**, ($p > 0.05$, n = 17-18). Preference index values of the mock control group (grey bars) were compared to groups trained with GA CS+ (blue bar) or cVA CS+ (red bar). Multiple comparisons are tested throughout this study with one-way ANOVA with Bonferroni correction. Significance level is set at $p < 0.05$. *$p < 0.05$, ****$p < 0.0001$. In this and all other bar graphs, bars and error bars indicate mean and SEM, respectively. **(C, G, K)** MG volume is defined by the area enwrapped by the postsynaptic densities of KC dendrites. MG lumen volume **(D, H, L)** is the volume of the lumen as defined in Figure 1F. In STM the relative volume of DA1- MGs **(C)** and of their lumen **(D)** is not different between groups ($p > 0.05$; n = 15-20). In LTM the MG volume **(G)** and the lumen volume **(H)** of DA1- MGs in flies trained with cVA CS+ are smaller than in flies from the mock

184 control group or of flies trained with GA CS+ (* p < 0.05, **p < 0.01; *n* = 19–25). **(E, I, M)**
185 Number of DA1-PN positive MGs is unaffected in STM **(E)** (*p* > 0.05; n = 18 – 24). In LTM,
186 number of DA1-PN positive MGs in cVA CS+ trained flies is higher compared to flies of the
187 mock control or GA CS+ group **(I)** (*p < 0.05; n = 18-24)**. (K-L)** The structural modifications of
188 DA1- MGs in cVA CS+ trained flies after the appetitive LTM protocol were suppressed in *rut*
189 mutants (*p* > 0.05, n = 13–21). In all box plots in this and the following figures, the edges of
190 the boxes are the first and third quartiles, thick lines mark the medians, and whiskers
191 represent data range.

192

193 The increase in DA1-PN positive MG number after LTM formation with cVA CS+
194 suggests that new boutons might be formed during consolidation. To gain insight into
195 the cellular fundamentals of these modifications, we expressed in DA1-PN axons the
196 membrane-tagged fluorescent protein *UAS-GAP43::Venus* together with *UAS-brp-*
197 *short*^{cherry} and highlighted the postsynaptic densities on KC dendrites using *MB247-*
198 *Dα7::GFP* (Figure 3A-D). Serial optical sections of the MBCs of these flies trained
199 with cVA CS+, with GA CS+ or in the mock paradigm (Figure S2H) were used to
200 generate 3D reconstructions that were then aligned to a reference brain (JFRC2
201 [50]). The DA1-PN axons were then traced in the aligned high-resolution scans of the
202 MBC (Figure 3E). The DA1-PN boutons were highly clustered in the dorsal-posterior
203 part of the calyx [51], supporting the view that the localization within the MBC of DA1-
204 PN boutons is not entirely random (Figure 3F) [52]. The total length of DA1-PN
205 collaterals measured from the point where they leave the inner antennocerebral tract
206 (iACT) was increased in flies that had formed LTM after cVA CS+ training compared
207 to mock-control flies (Figure 3G). In addition, the total fraction of the MBC volume
208 containing DA1-PN positive boutons was increased in flies that had formed cVA CS+
209 LTM (Figure 3H). These observations suggest that during consolidation, additional
210 boutons are created by local growth at existing DA1-PN collaterals (Figure 3I).

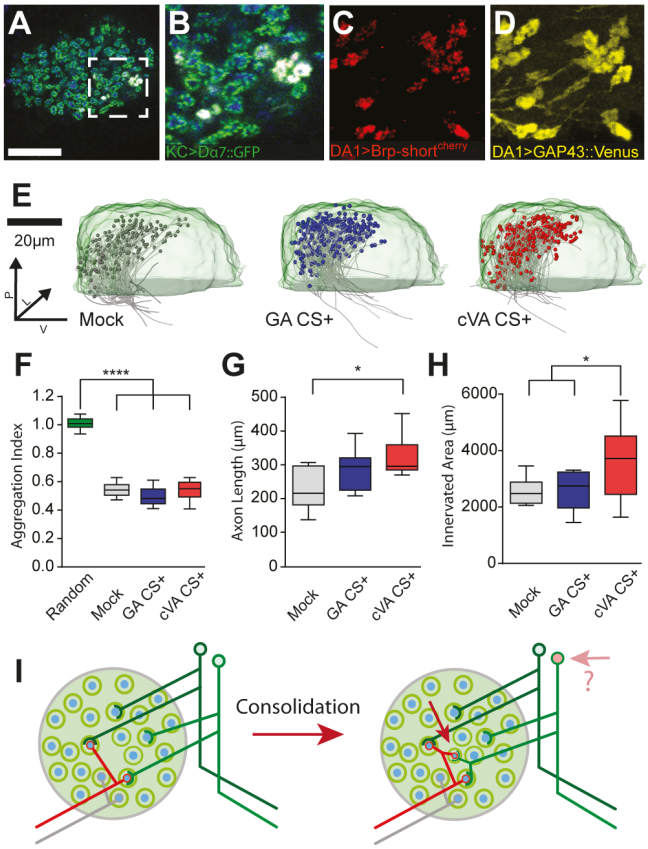

211

212 **Figure 3 | Modifications of axon collaterals and wiring properties of projection**
213 **neurons within the mushroom body calyx after long-term memory formation**

214 **(A)** Single optical section of the MBC of flies expressing Dα7GFP (green) in the KCs and
215 Brp-short^{cherry} (red) plus GAP43-Venus (yellow) in DA1-PNs (*R37H08-Gal4*); PN boutons
216 (blue; anti-Synapsin antibodies). **(B-D)** Magnification of the white square in (A) displaying the
217 merge as in A **(B)** or a maximum-intensity projection of Brp-short^{cherry} **(C)** or of GAP43-Venus
218 **(D)** signals. **(E)** Medial view of registered PN axons (grey) with traced boutons (grey, blue,
219 red spheres) within a standard calyx (light green). The registered PN traces are of mock
220 (grey), GA CS+ (blue) or cVA CS+ (red) trained groups. n = 10 for each group. **(F)** Boutons
221 are highly clustered independently of the treatment (Clark and Evans Aggregation index
222 compared to a hypothetical random distribution; ****$p < 0.0001$). **(G)** Total collateral axons
223 length of mock control, GA CS+ or cVA CS+ flies. (*$p < 0.05$; n = 10). **(H)** The convex hull
224 volume containing all DA1-boutons in the MBC per condition is increased in cVA CS+ flies
225 compared to mock control and GA CS+ group. **(I)** We suggest that the increased number of
226 MGs after consolidation is due to the formation of additional boutons responding to cVA. The
227 additional boutons form full MGs, as postsynaptic profiles of KCs surround them. It is unclear
228 whether this reorganization might lead to the recruitment of additional responding KCs (see
229 Discussion).

230

231 To address whether the observed structural changes within the MGs after LTM

232 impact on the functional representation of the CS in the MBC we analysed calcium

233 dynamics in KC dendrites. For this, we utilized flies carrying *MB247-homer::GCaMP3*

234 [30] in combination with volumetric calcium imaging (Figure 4A). We utilized this
235 simple genotype to guarantee that flies performed well in LTM experiments (Figure
236 S2I). We measured calcium response in the entire MBC volume during a single
237 odour application (5 s odour stimulation) of either cVA (1:400 in 5% EtOH) or EtOH
238 alone (5%). To identify areas with increased calcium dynamics during odour
239 stimulation we overlaid a grid consisting of 5x5 μm^2 ROIs over each optical section of
240 the volumetric time series. Based on the grid segmentation, we then calculated the
241 average $\Delta F/F\%$ for each ROI in the MBC. ROIs were classified as odour responsive
242 if the measured calcium response exceeded a set threshold ($\Delta F/F\% > 3x$ standard
243 deviation) during the first 2 s of stimulation (Figure 4B, C; Figure S3A, B). The
244 response pattern elicited specifically by cVA was defined after subtraction of the
245 EtOH response (Figure 4C; Figure S3C, D; see also Figure 1C). This approach
246 yielded a comprehensive picture of the functional odour response over time in the
247 MBC of trained or control flies (Figure S3D, E). After appetitive LTM formation, the
248 percentage of cVA-responsive ROIs was increased in cVA CS+ flies compared to the
249 mock control (Figure 4D) ($n = 7$, $p < 0.05$), suggesting that the additional DA1-PN
250 boutons are functionally connected to their postsynaptic KC counterparts and
251 capable of initiating a response in the postsynaptic KCs. We further analysed the
252 calcium dynamics over time of all animals of the mock or cVA CS+ group (Figure 4E,
253 F). Linear regression analysis of the fluorescence change during odour stimulation
254 showed a steeper drop of the linear fit in cVA CS+ flies ($R^2 = 0.6429$) towards
255 baseline compared to flies of the mock control group ($R^2 = 0.1124$). Besides, the
256 response towards the odour was more variable in mock-trained flies compared to the
257 cVA CS+ flies (Figure S3F). Initially (0-4s after start of stimulation), the total response
258 towards cVA stimulation was indistinguishable between mock control and cVA CS+

group. However, at subsequent time points (4-7s after start of stimulation) responses were significantly lower in KC dendrites of the cVA CS+ group compared to the mock control, showing a faster calcium decay towards the trained odour in CS+ flies (n = 7, $p < 0.05$) (Figure S3G). Together, these data indicate a temporal sharpening of the odour response.

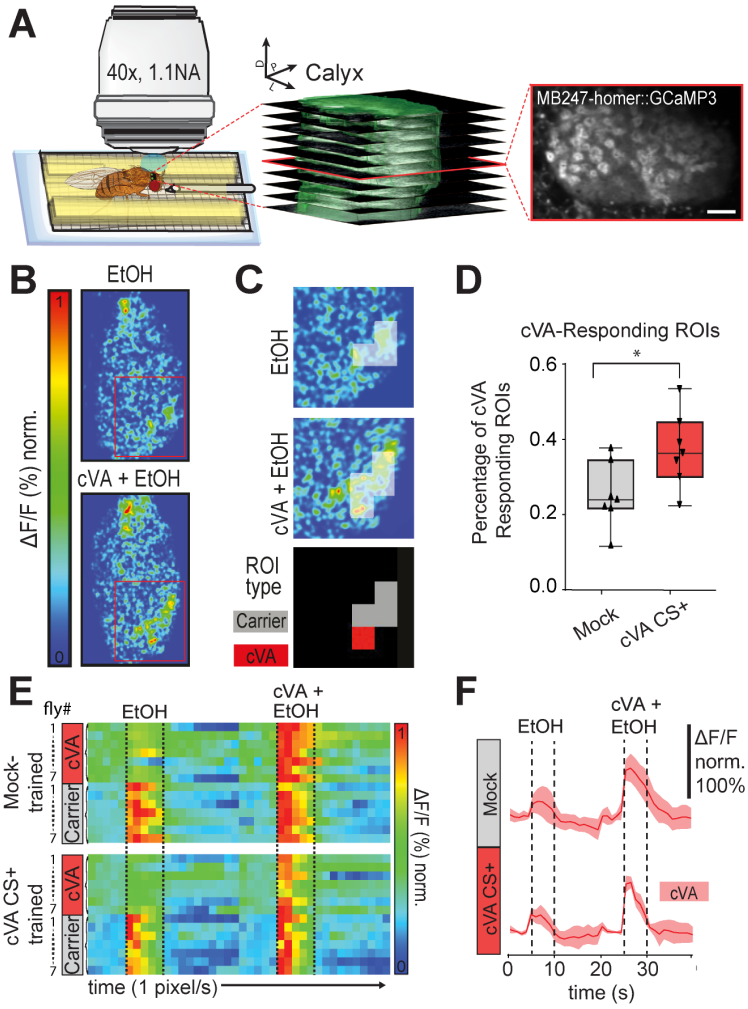

Figure 4 | Long-term memory-induced functional plasticity in the mushroom body calyx

(A) Two-photon *in vivo* imaging setup. Schematic of a fly placed on a custom-made holder under a two-photon microscope equipped with a 40x 1.1 NA water immersion objective. The odour is delivered for 5s with a moisturized, constant air stream through a 1.2mm cannula. (Central panel) Z series of the entire MBC volume of flies expressing post-synapse-tagged Homer-GCaMP3 imaged during odour application at 1Hz (10 optical sections per volume, 4µm step size). (Right panel) A single slice of the image stack shown in the middle panel.

273 Scale bar = 10 µm. **(B)** Representative optical section from a volumetric time series showing
274 false-coloured response of KC dendrites to 5 s exposure to EtOH (top) or cVA + EtOH
275 (bottom). **(C)** Magnification of the red square area in (B). 5x5 μm^2 ROIs were classified as
276 cVA-responsive (red) if they were only active during cVA + EtOH application, but did not
277 respond to EtOH alone. **(D)** The percentage of cVA responsive ROIs increased after LTM
278 acquisition compared to the mock control (*$p < 0.05$; n = 7). **(E)** Dynamics of ΔF/F% changes
279 over time in KCs of *MB247-homer::GCaMP3* flies after mock training (top) or LTM acquisition
280 (bottom). Each row of the heat map represents average responses per animal of all cVA
281 responsive ROIs (pink) or of all carrier EtOH responsive ROIs (grey) within one MBC over
282 time. Each column represents one 1s. Flies are first exposed to the EtOH (5s) and then to
283 cVA + EtOH (5s) as indicated by the dashed lines. **(F)** Plot of average calcium dynamics over
284 time of cVA responsive ROIs during 5 s stimulation with EtOH or with cVA in EtOH (dashed
285 lines) in mock-trained (top) or cVA CS+ (bottom) flies (n = 7 per condition).

286 **Discussion**

287 We report input-specific reorganization of the adult MBC circuit associated with the
288 formation of long-term appetitive memory. By visualizing presynaptic markers in PNs
289 and the KC postsynaptic densities, we uncover an increase in the number of PN
290 boutons and at the same time reveal that these boutons are enveloped by KC
291 postsynaptic profiles, suggesting that new MGs are formed during memory
292 consolidation. These findings are particularly remarkable, given the high degree of
293 complexity of the MG microcircuits revealed by our EM reconstruction and including
294 the dendrite claws of multiple KCs of distinct subtypes. The cellular mechanisms
295 leading to the increased number of odour-specific complex MGs remain to be
296 clarified, but they will require a tight coordination between pre- and postsynaptic
297 partners. We suggest that they could be driven by intrinsic reactivation of KCs during
298 the consolidation phase [53, 54] or by modulatory inputs into the calyx [38, 55-58]. In
299 either case, we expect a complex pattern of activation that might be difficult to
300 reproduce in artificial settings [29, 59]. In agreement with our present report, the
301 density of PN boutons in the MBC increases after appetitive long-term conditioning in
302 honeybees and transiently also after avoidance learning in leaf-cutting ants [60, 61].
303 In comparison to those data, using genetic and functional identification of PN subsets

304 we reveal here that the structural modifications are specific and limited to the PNs
305 conveying the conditioned odour. Importantly, our *in vivo* functional imaging data
306 support the view that the circuit reorganization that we describe leads to additional
307 functional MGs responding to the conditioned odour. Additionally, they demonstrate a
308 specific change in functional response in the KC dendrites towards the trained odour
309 as the calcium levels drop faster towards baseline after appetitive associative
310 conditioning. The faster decay kinetics could contribute to a more efficient temporal
311 summation of responses or refine the KC response [62]. They are in line with recent
312 data from appetitive conditioning experiments from the honeybee possibly rooted in
313 inhibitory modifications [63]. An important open question is the effect of the increased
314 number of responding MGs on the pattern of KC activation. KCs respond sparsely to
315 odour input and require the coincident activation of multiple of their claws to produce
316 an action potential [64]. Our data might underlie the addition of connections between
317 the active PNs and, preferentially, a set of already responding KCs, leading to
318 facilitated response to the conditioned odour, but without changing the set of
319 responding KCs. A recent publication suggests an exciting alternative view. After
320 aversive LTM establishment, the number of KCs responding to the conditioned odour
321 is increased [65]. If we hypothesize that appetitive conditioning could lead to a similar
322 outcome, our data could provide anatomical and functional support to these findings.
323 The combination of these data suggests that the pattern of KC response is
324 modulated by experience during the adult life of the animal and might represent a
325 rich signifier of sensory stimulus and context.

326 **Acknowledgements**

We thank K. Keppler, M. Schoelling, A. Mueller and J. C. Vijayakumar for technical assistance. We are grateful to C.B. Fisher, S.A. Calle-Schuler, N. Sharifi, B. Gorko, L. Kmecova, I.J. Ali, N. Masoodpanah, J. Hsu and F. Li in D. D. Bock's lab for their support in tracing evaluation. We thank Y. Aso, HHMI Janelia, the Kyoto Drosophila Genetic Resource Center and the Bloomington Stock Center for fly lines and FlyBase. We are grateful for their assistance to C. Moehl in the establishment of the cluster analysis, S. Dipt with initial calcium imaging experiments and R. Court for providing the brain aligner and support. We thank S. Sachse, D. Isbrandt, T. Hige, S. Remy, M. Nawrot, O. Barnstedt, the members of the Tavosanis lab for discussion and/or critical reading of the manuscript and B. Schaffran for help with video editing. L.B. acknowledges support by the Bonn International Graduate School of Neuroscience. This work was supported by the DFG FOR 2705 to G.T.

Author Contributions

L.B. and G.T. conceived the project and designed the experiments. L.B., P.R. and L.P. constructed fly strains, performed behavioural experiments, produced and analysed the anatomical data. J.S.L. and D.D.B. established the set of EM data and P.R. performed the tracings presented here. Scripts and routines for the analysis were established by L.B. and L.P. Functional imaging experiments were designed and performed by L.B and L.P. with support by A.F. The manuscript was written by G.T, L.B., P.R and L.P.

Competing Financial Interests statement

The authors declare no competing interests.

349 **Methods**

350 **EM reconstruction and identification**

351 Neuron skeletons were reconstructed in a serial section transmission electron
352 microscope (ssTEM) volume of a complete female adult *Drosophila melanogaster*
353 brain [37] and manually traced using CATMAID [66]. Thus, traced neuron skeletons
354 represent the branching of neurons and the location of their cell bodies and
355 synapses. Chemical synapses were manually annotated and identified consistently
356 with the criteria of other CATMAID-based *Drosophila* connectomic studies [37]: 1) an
357 active zone (AZ) surrounded by vesicles, 2) a presynaptic specialization (*e.g.* T-bar),
358 3) synaptic cleft and 4) a post synaptic density zone (PSD), which however can be
359 absent. If the PSD is absent, we annotated all cells along the synaptic cleft as
360 postsynaptic [37, 67]. Neuron identity is based on previously described morphologies
361 in light microscopy (KC subtypes, APL, MB-C1, PN), such as dendritic branching,
362 axonal projection and location in the neuropil [38, 40, 52, 68, 69]. Additionally, we
363 performed a neuron search against a light microscopy dataset in NBLAST [70], as
364 described in [37] for PN subtype identification. 3D reconstructions of the PN bouton
365 and KC claws from ssTEM sections were created manually with the ImageJ plugin
366 TrakEM2 [71].

367 **Fly strains**

368 Flies were raised at 25°C, 60% relative humidity in a 12h/12h light-dark cycle on a
369 standard cornmeal-based diet. Individual insertions are listed below. Detailed
370 information on genotypes used in this study is listed in the Supplemental Genotypes
371 and Statistics table.

372

Insertion	Source	Reference
R37H08-Gal4	Kind gift of Y. Aso, HHMI, Janelia	FlyBase: FBti0191253
P{UASp-Venus.GAP43}10	Bloomington Drosophila Stock center	FlyBase: FBti0129930

P{UAS-tdTom.S}2	Bloomington Drosophila Stock center	FlyBase: FBti0145103
P{ry[+t7.2]=IArB}rut[2080]	Kind gift of A. Fiala, Uni Goettingen	[49] FlyBase: FBti0003267
P{UAS-GCaMP3.homer}	Kind gift of A. Fiala, Uni Goettingen	[30]
MB247-Dα7::GFP	Lab stock collection	[29]
UAS-brp-short^{cherry}	Lab stock collection	[29]

373

374 **Behaviour**

375 All experimental steps were performed at 23°C, 60% relative humidity using mixed
376 populations of *Drosophila* males and females maintained in a 12h/12h light/dark
377 cycle. Flies were collected 0-4d after eclosion, starved for 24 hours on wet paper
378 tissue (Kimberly-Clark Worldwide Inc.) allowing for water uptake and then trained. In
379 appetitive memory experiments ~80 flies were first exposed to an odour (CS-) alone
380 (2min in short- and 5 minutes in long-term memory experiments). After a 2min inter-
381 stimulus pause flies were trained by receiving dry sucrose on filter paper (3M Chr,
382 Whatman) paired with a second odour (CS+) (2min in short- and 5 minutes in long-
383 term memory experiments). 5 minutes of sugar availability improved the survival of
384 flies undergoing the LTM paradigm. In mock controls, all stimuli used in the
385 associative conditioning experiment were presented separately. Flies were tested
386 after 1min retention time for short- or after 24h retention time for long-term memory.
387 During the 24h retention flies were deprived of food and maintained in tubes
388 containing moist paper tissue. During the test flies were allowed to choose between
389 CS+ and CS- odours in a T-maze for 2min. A preference index (PI) was then
390 calculated as the ratio of the difference between the number of flies that chose the
391 CS+ and those that chose the CS- odour and the total number of flies: $PI =$
392 $\frac{(CS+)-(CS-)}{(CS+)+(CS-)}$. Odours used for conditioning were 11-cis vaccenyl acetate (Cayman

393 Chemicals) 1:400 in 5% EtOH in PBS, geranyl acetate (Sigma Aldrich) 1:100 in 5%
394 EtOH in PBS or 5% EtOH in PBS. EtOH was necessary to provide a food-related
395 context to the starved flies (Figure S2B).

396 **De-novo protein synthesis inhibition**

397 Immediately after training, flies were fed 35 mM cycloheximide (Sigma-Aldrich) [6]
398 dissolved in 125mM sucrose and 0.01% carmine solution for 30min. The red dye
399 carmine allowed confirming rapid drug uptake. A control group fed with 125mM
400 sucrose and 0.01% carmine (Sigma-Aldrich) solution showed no learning defects.

401 **Immunohistochemistry**

402 2-5 flies were randomly picked from conditioning experiments right before testing.
403 Brains of females were dissected in cold phosphate-buffered saline (PBS) with 0.05%
404 Triton and subsequently fixed in PBS containing 4% formaldehyde at RT for 50 min.
405 After fixation brains were washed in PBS with 0.3% Triton before incubation
406 overnight at 4°C with the following primary antibodies all diluted in PBS with 0.3%
407 Triton: rabbit anti-RFP (1:2000; Rockland), rabbit anti-GFP (1:200; Life
408 Technologies), mouse monoclonal anti-synapsin (3C11, 1:100; DSHB), mouse
409 monoclonal anti-β-Galactosidase (1:200 Abcam). After washing, the brains were
410 incubated with secondary antibodies in PBS containing 0.3% Triton for 4h at RT.

411 The secondary antibodies were Alexa Fluor568-conjugated goat anti-rabbit, Alexa
412 Fluor488-conjugated goat anti-rabbit, Alexa Fluor568-conjugated goat anti-mouse,
413 Alexa Fluor633-conjugated goat anti-mouse (all used 1:200 and from Life
414 Technologies). Brains were mounted in Vectashield (Vector) and imaged with a laser
415 scanning confocal microscope (LSM 780, Zeiss). For high resolution scans we used
416 a C Plan-Apochromat 63x/1,4 Oil objective (Zeiss) with a voxel size of
417 0.09x0.09x0.25μm^3 for quantitative analysis. Overviews of entire brains were taken
418 with an LCI Plan-Apochromat 25x/0.8 objective (Zeiss) at a voxel size of
419 0.55x0.55x1μm^3.

420 **Axon reconstruction**

421 To analyse axon and bouton distribution in the calyx, membrane-tagged Venus was
422 expressed in addition to the previously used markers under the control of a DA1-PN
423 Gal4-driver line (*R37H08-GAL4, UAS-Gap43::Venus / MB247-Dα7::GFP, UAS-brp-*
424 *short*^{cherry}). Brains of 10 female flies per condition were immunolabelled with anti-
425 synapsin antibodies (as above) and imaged. For PN axon reconstruction a high-
426 resolution scan (0.09x0.09x0.25µm^3, 63x NA1.4 oil immersion) of the right brain
427 hemisphere of female flies was acquired with a confocal microscope. In addition, an
428 overview scan used for registration was taken with a low magnification objective (25x;
429 NA 0.8 multi-immersion). PN axon reconstruction was performed on the high-
430 resolution scan of Venus signal in the trees toolbox available for Matlab [72]. In a
431 second step tracings and high-resolution images were aligned to the registered calyx.
432 For generation of a standard calyx with a volume of 37583 µm^3 (Figure 3E, light
433 green) the Dα7 signal of three registered calyces was averaged and reconstructed in
434 Amira using the segmentation editor. Next, tracings were aligned to the registered
435 overview scan in two steps. First, the iACT of the high-resolution image and of the
436 registered brain in the Venus channel were aligned. Next, the calyx volume of the
437 high-resolution calyx and the standard calyx went through a rigid registration
438 performed in Amira. The alignment parameters were then applied to the axon
439 reconstructions. Boutons were traced on the now registered high-resolution images
440 with the landmark function in Amira. Bouton distribution inside the MBC was
441 evaluated within a 3D grid of 10µm^3 cubes.

442 **Two-photon *in vivo* calcium imaging**

443 A mixed population of up to 4 d old *MB247-homer::GCaMP3* flies were starved for
444 18h at 22°C before appetitive conditioning with cVA (1:400, 5% EtOH in PBS), GA
445 (1:100, 5% EtOH in PBS) was used as CS-. Starved untrained flies displayed no bias
446 towards either of these odours at 24 hours. Flies used for imaging were randomly
447 picked from the trained group right before testing. They were used for imaging only if
448 the remaining flies from the same group had learned. For imaging, flies were briefly
449 anesthetized on a peltier element at 4°C, placed into a custom-built imaging chamber
450 (Figure 4A) and fixed using adhesive tape. The head capsule was opened under
451 Ringer´s solution (5 mM HEPES, pH 7.4, 130 mM NaCl, 5 mM KCl, 2 mM $CaCl_2$, 2
452 mM $MgCl_2$). To minimize movement brains were stabilized with 1,5% low melting

453 agarose (Thermo Scientific) in Ringer´s solution. Flies were imaged with a two-
454 photon laser-scanning microscope (LaVision BioTec, TriM Scope II) equipped with an
455 ultra-fast z-motor (PIFOC® Objective Scanner Systems 100µm range) and a Zeiss
456 C-Apochromat 40x, 1.1 NA water –immersion objective. Two-photon images were
457 analysed using Fiji/ImageJ [73]. GCaMP fluorescence was excited at 920 nm using a
458 Ti:sapphire laser (Coherent Chameleon). A stack consisting of ~ 10 optical sections
459 was taken at 1Hz in approximately 0,26x0,26µm xy- and at 4µm z- resolution. Odours
460 were applied with a constant humidified air stream (10ml/s) using a commercial
461 device (Stimulus Controller CS 55, Ockenfels SYNTECH GbmH) triggered 5s after
462 acquisition of the 1st frame by a multifunction I/O module (NI USB-6008), which was
463 controlled by Matlab (Data Acquisition Toolbox). To record DA1 neurons specific
464 responses, *UAS-tdTomato; R37H08-GAL4, MB247-Homer::GCaMP3* flies were
465 anesthetized on ice, positioned in a polycarbonate imaging chamber ([74]; gift from S.
466 Tomchik), and immobilized using Myristic Acid (Sigma-Aldrich). To allow optical
467 access to the Calyx, a small window was opened through the head capsule under
468 Ringer´s solution. Two-photon microscopy was conducted as described above.

469 **Two-photon image data processing**

470 The time series was processed with a custom Fiji/ ImageJ macro and corrected for
471 small x/y shifts with the StackReg plug-in [75]. A grid (ROIs, side length 5 µm) was
472 assigned for each optical slide of a stack covering the entire calyx. Intensity tables of
473 each square of the grid were exported to Microsoft Excel and the ΔF/F was
474 calculated. The baseline (F_0) was set by averaging the intensities within each ROI of
475 the 5 frames prior to odour stimulation. ROIs were regarded as responsive, if their
476 normalized ΔF/F% throughout the first 2s of odour application exceeded 3x the
477 standard deviation of the F_0 of the same ROI in the 5s (=5 images) before odour
478 stimulation. ROIs below that threshold were assigned into the category
479 “unresponsive”. ROIs calcium responses higher than the threshold were further
480 subdivided into three categories. The first category was “Carrier” (responsive to both,
481 5% EtOH and 1:400 cVA, 5% EtOH). The second category was “cVA” (responsive
482 only to 1:400 cVA, 5% EtOH and not to 5% EtOH) or “EtOH” (response only to 5%
483 EtOH application and not to 1:400 cVA, 5% EtOH). To analyse DA1 boutons
484 responses to 5% EtOH and 1:400 cVA+ 5% EtOH were recorded from naïve *UAS-*

485 *tdTomato; R37H08-GAL4, MB247-Homer::GCaMP3* flies, exported to Fiji/ ImageJ
486 and ROIs were manually drawn around DA1 boutons based on the tdTomato
487 fluorescence. Intensity values of each ROI were transferred to Microsoft Excel and
488 ΔF/F values were calculated using the average of the first 5 frames prior to odour
489 stimulation as baseline (F_0). Responsive ROIs were defined as above. These results
490 were age, gender and sequence independent as presenting the odours in a different
491 order did not change the results of the analysis. Calcium traces were generated in
492 Prism 7 (GraphPad Software).

493 **Statistics**

494 Statistical analyses were performed with Prism7.01 software (GraphPad). All data
495 were tested for normality (D'Agostino & Pearson omnibus normality test) and
496 homogeneity of variances (F-test). Comparisons of normally distributed data were
497 tested by a one-sample t test, a two-sample t test or one-way analysis of variance
498 (ANOVA) followed by planned, pairwise multiple-comparison tests with adjusted p-
499 values (Bonferroni), as shown in the Genotypes and Statistics table. Definition of
500 statistical significance was set to <0.05. Asterisks denote * $p<0.05$; ** $p<0.01$;
501 ***$p<0.001$; **** $p<0.0001$; n.s. not significant.

502 **References**

503 1. Josselyn, S.A., and Tonegawa, S. (2020). Memory engrams: Recalling the past and
504 imagining the future. Science *367*.

505 2. Boto, T., Stahl, A., and Tomchik, S.M. (2020). Cellular and circuit mechanisms of
506 olfactory associative learning in Drosophila. Journal of neurogenetics *34*, 36-46.

507 3. Wang, Y., Mamiya, A., Chiang, A.-s., and Zhong, Y. (2008). Imaging of an early
508 memory trace in the Drosophila mushroom body. The Journal of neuroscience : the
509 official journal of the Society for Neuroscience *28*, 4368-4376.

510 4. Liu, C., Placais, P.Y., Yamagata, N., Pfeiffer, B.D., Aso, Y., Friedrich, A.B., Siwanowicz,
511 I., Rubin, G.M., Preat, T., and Tanimoto, H. (2012). A subset of dopamine neurons
512 signals reward for odour memory in Drosophila. Nature *488*, 512-516.

513 5. Burke, C.J., Huetteroth, W., Owald, D., Perisse, E., Krashes, M.J., Das, G., Gohl, D.,
514 Silies, M., Certel, S., and Waddell, S. (2012). Layered reward signalling through
515 octopamine and dopamine in Drosophila. Nature *492*, 433-437.

516 6. Tully, T., Preat, T., Boynton, S.C., and Del Vecchio, M. (1994). Genetic dissection of
517 consolidated memory in Drosophila. Cell *79*, 35-47.

518 7. Bailey, C.H., Bartsch, D., and Kandel, E.R. (1996). Toward a molecular definition of
519 long-term memory storage. Proc Natl Acad Sci U S A *93*, 13445-13452.

520 8. Dubnau, J., and Chiang, A.S. (2013). Systems memory consolidation in Drosophila.
521 Curr Opin Neurobiol *23*, 84-91.

522 9. Cervantes-Sandoval, I., Martin-Pena, A., Berry, J.A., and Davis, R.L. (2013). System-like
523 consolidation of olfactory memories in Drosophila. J Neurosci *33*, 9846-9854.

524 10. Kitamura, T., and Ogawa, S.K. (2017). Engrams and circuits crucial for systems
525 consolidation of a memory. *356*, 73-78.

526 11. Caroni, P., Donato, F., and Muller, D. (2012). Structural plasticity upon learning:
527 regulation and functions. Nat Rev Neurosci *13*, 478-490.

528 12. Holtmaat, A., and Caroni, P. (2016). Functional and structural underpinnings of
529 neuronal assembly formation in learning. Nat Neurosci *19*, 1553-1562.

530 13. Kleim, J.A., Freeman, J.H., Jr., Bruneau, R., Nolan, B.C., Cooper, N.R., Zook, A., and
531 Walters, D. (2002). Synapse formation is associated with memory storage in the
532 cerebellum. Proc Natl Acad Sci U S A *99*, 13228-13231.

533 14. Hihara, S., Notoya, T., Tanaka, M., Ichinose, S., Ojima, H., Obayashi, S., Fujii, N., and
534 Iriki, A. (2006). Extension of corticocortical afferents into the anterior bank of the
535 intraparietal sulcus by tool-use training in adult monkeys. Neuropsychologia *44*,
536 2636-2646.

537 15. Bassett, D.S., Wymbs, N.F., Porter, M.A., Mucha, P.J., Carlson, J.M., and Grafton, S.T.
538 (2011). Dynamic reconfiguration of human brain networks during learning. Proc Natl
539 Acad Sci U S A *108*, 7641-7646.

540 16. Gu, S., Pasqualetti, F., Cieslak, M., Telesford, Q.K., Yu, A.B., Kahn, A.E., Medaglia, J.D.,
541 Vettel, J.M., Miller, M.B., Grafton, S.T., et al. (2015). Controllability of structural brain
542 networks. Nat Commun *6*, 8414.

543 17. Maviel, T., Durkin, T.P., Menzaghi, F., and Bontempi, B. (2004). Sites of neocortical
544 reorganization critical for remote spatial memory. Science (New York, N.Y.) *305*, 96-
545 99.

546 18. Chklovskii, D.B., Mel, B.W., and Svoboda, K. (2004). Cortical rewiring and information
547 storage. Nature *431*, 782-788.

548 19. Gogolla, N., Galimberti, I., and Caroni, P. (2007). Structural plasticity of axon
549 terminals in the adult. Curr Opin Neurobiol *17*, 516-524.

550 20. Bennett, S.H., Kirby, A.J., and Finnerty, G.T. (2018). Rewiring the connectome:
551 Evidence and effects. Neurosci Biobehav Rev *88*, 51-62.

552 21. Boele, H.J., Koekkoek, S.K., De Zeeuw, C.I., and Ruigrok, T.J. (2013). Axonal sprouting
553 and formation of terminals in the adult cerebellum during associative motor learning.
554 J Neurosci *33*, 17897-17907.

555 22. Chen, J.L., Margolis, D.J., Stankov, A., Sumanovski, L.T., Schneider, B.L., and
556 Helmchen, F. (2015). Pathway-specific reorganization of projection neurons in
557 somatosensory cortex during learning. Nat Neurosci *18*, 1101-1108.

558 23. Poort, J., Khan, A.G., Pachitariu, M., Nemri, A., Orsolic, I., Krupic, J., Bauza, M., Sahani,
559 M., Keller, G.B., Mrsic-Flogel, T.D., et al. (2015). Learning Enhances Sensory and
560 Multiple Non-sensory Representations in Primary Visual Cortex. Neuron *86*, 1478-
561 1490.

562 24. Grewe, B.F., Grundemann, J., Kitch, L.J., Lecoq, J.A., Parker, J.G., Marshall, J.D., Larkin,
563 M.C., Jercog, P.E., Grenier, F., Li, J.Z., et al. (2017). Neural ensemble dynamics
564 underlying a long-term associative memory. Nature *543*, 670-675.

565 25. de Belle, J.S., and Heisenberg, M. (1994). Associative odor learning in Drosophila
566 abolished by chemical ablation of mushroom bodies. Science *263*, 692-695.

567 26. Butcher, N.J., Friedrich, A.B., Lu, Z., Tanimoto, H., and Meinertzhagen, I.A. (2012).
568 Different classes of input and output neurons reveal new features in microglomeruli
569 of the adult Drosophila mushroom body calyx. J Comp Neurol *520*, 2185-2201.

570 27. Caron, S.J., Ruta, V., Abbott, L.F., and Axel, R. (2013). Random convergence of
571 olfactory inputs in the Drosophila mushroom body. Nature *497*, 113-117.

572 28. Yasuyama, K., Meinertzhagen, I.A., and Schurmann, F.W. (2002). Synaptic
573 organization of the mushroom body calyx in Drosophila melanogaster. J Comp Neurol
574 *445*, 211-226.

575 29. Kremer, M.C., Christiansen, F., Leiss, F., Paehler, M., Knapek, S., Andlauer, T.F.,
576 Forstner, F., Kloppenburg, P., Sigrist, S.J., and Tavosanis, G. (2010). Structural long-
577 term changes at mushroom body input synapses. Curr Biol *20*, 1938-1944.

578 30. Pech, U., Revelo, N.H., Seitz, K.J., Rizzoli, S.O., and Fiala, A. (2015). Optical dissection
579 of experience-dependent pre- and postsynaptic plasticity in the Drosophila brain. Cell
580 Rep *10*, 2083-2095.

581 31. Leiss, F., Groh, C., Butcher, N.J., Meinertzhagen, I.A., and Tavosanis, G. (2009).
582 Synaptic organization in the adult Drosophila mushroom body calyx. J Comp Neurol
583 *517*, 808-824.

584 32. Datta, S.R., Vasconcelos, M.L., Ruta, V., Luo, S., Wong, A., Demir, E., Flores, J.,
585 Balonze, K., Dickson, B.J., and Axel, R. (2008). The Drosophila pheromone cVA
586 activates a sexually dimorphic neural circuit. Nature *452*, 473-477.

587 33. Kurtovic, A., Widmer, A., and Dickson, B.J. (2007). A single class of olfactory neurons
588 mediates behavioural responses to a Drosophila sex pheromone. Nature *446*, 542-
589 546.

590 34. Schlief, M.L., and Wilson, R.I. (2007). Olfactory processing and behavior downstream
591 from highly selective receptor neurons. Nat Neurosci *10*, 623-630.

592 35. Lebreton, S., Grabe, V., Omondi, A.B., Ignell, R., Becher, P.G., Hansson, B.S., Sachse,
593 S., and Witzgall, P. (2014). Love makes smell blind: mating suppresses pheromone
594 attraction in Drosophila females via Or65a olfactory neurons. Sci Rep *4*, 7119.

595 36. Lebreton, S., Trona, F., Borrero-Echeverry, F., Bilz, F., Grabe, V., Becher, P.G.,
596 Carlsson, M.A., Nässel, D.R., Hansson, B.S., Sachse, S., et al. (2015). Feeding regulates
597 sex pheromone attraction and courtship in Drosophila females. Scientific Reports *5*,
598 13132.

599 37. Zheng, Z., Lauritzen, J.S., Perlman, E., Robinson, C.G., Nichols, M., Milkie, D., Torrens,
600 O., Price, J., Fisher, C.B., Sharifi, N., et al. (2018). A Complete Electron Microscopy
601 Volume of the Brain of Adult Drosophila melanogaster. Cell *174*, 730-743 e722.

602 38. Aso, Y., Hattori, D., Yu, Y., Johnston, R.M., Iyer, N.A., Ngo, T.T., Dionne, H., Abbott,
603 L.F., Axel, R., Tanimoto, H., et al. (2014). The neuronal architecture of the mushroom
604 body provides a logic for associative learning. Elife *3*, e04577.

605 39. Lin, H.H., Lai, J.S., Chin, A.L., Chen, Y.C., and Chiang, A.S. (2007). A map of olfactory
606 representation in the Drosophila mushroom body. Cell *128*, 1205-1217.

607 40. Liu, X., and Davis, R.L. (2009). The GABAergic anterior paired lateral neuron
608 suppresses and is suppressed by olfactory learning. Nat Neurosci *12*, 53-59.

609 41. Schmid, A., Hallermann, S., Kittel, R.J., Khorramshahi, O., Frolich, A.M., Quentin, C.,
610 Rasse, T.M., Mertel, S., Heckmann, M., and Sigrist, S.J. (2008). Activity-dependent
611 site-specific changes of glutamate receptor composition in vivo. Nat Neurosci *11*,
612 659-666.

613 42. Tempel, B.L., Bonini, N., Dawson, D.R., and Quinn, W.G. (1983). Reward learning in
614 normal and mutant Drosophila. Proc Natl Acad Sci U S A *80*, 1482-1486.

615 43. Bhandawat, V., Olsen, S.R., Gouwens, N.W., Schlief, M.L., and Wilson, R.I. (2007).
616 Sensory processing in the Drosophila antennal lobe increases reliability and
617 separability of ensemble odor representations. Nat Neurosci *10*, 1474-1482.

618 44. Pohl, J.B., Baldwin, B.A., Dinh, B.L., Rahman, P., Smerek, D., Prado, F.J., Sherazee, N.,
619 and Atkinson, N.S. (2012). Ethanol preference in Drosophila melanogaster is driven
620 by its caloric value. Alcoholism, clinical and experimental research *36*, 1903-1912.

621 45. Levin, L.R., Han, P.L., Hwang, P.M., Feinstein, P.G., Davis, R.L., and Reed, R.R. (1992).
622 The Drosophila learning and memory gene rutabaga encodes a Ca2+/Calmodulin-
623 responsive adenylyl cyclase. Cell *68*, 479-489.

624 46. Thum, A.S., Jenett, A., Ito, K., Heisenberg, M., and Tanimoto, H. (2007). Multiple
625 memory traces for olfactory reward learning in Drosophila. J Neurosci *27*, 11132-
626 11138.

627 47. Lagasse, F., Devaud, J.M., and Mery, F. (2009). A switch from cycloheximide-resistant
628 consolidated memory to cycloheximide-sensitive reconsolidation and extinction in
629 Drosophila. J Neurosci *29*, 2225-2230.

630 48. Davis, R.L. (2011). Traces of Drosophila memory. Neuron *70*, 8-19.

631 49. Han, P.L., Levin, L.R., Reed, R.R., and Davis, R.L. (1992). Preferential expression of the
632 Drosophila rutabaga gene in mushroom bodies, neural centers for learning in insects.
633 Neuron *9*, 619-627.

634 50. Jenett, A., Rubin, G.M., Ngo, T.T., Shepherd, D., Murphy, C., Dionne, H., Pfeiffer, B.D.,
635 Cavallaro, A., Hall, D., Jeter, J., et al. (2012). A GAL4-driver line resource for
636 Drosophila neurobiology. Cell Rep *2*, 991-1001.

637 51. Clark, P.J., and Evans, F.C. (1954). Distance to nearest neighbour as a measure of
638 spatial relationships in populations. Ecology *35*, 445-453.

639 52. Jefferis, G.S., Potter, C.J., Chan, A.M., Marin, E.C., Rohlfing, T., Maurer, C.R., Jr., and
640 Luo, L. (2007). Comprehensive maps of Drosophila higher olfactory centers: spatially
641 segregated fruit and pheromone representation. Cell *128*, 1187-1203.

642 53. Ichinose, T., Aso, Y., Yamagata, N., Abe, A., Rubin, G.M., and Tanimoto, H. (2015).
643 Reward signal in a recurrent circuit drives appetitive long-term memory formation.
644 Elife *4*, e10719.

645 54. Cognigni, P., Felsenberg, J., and Waddell, S. (2018). Do the right thing: neural network
646 mechanisms of memory formation, expression and update in Drosophila. Curr Opin
647 Neurobiol *49*, 51-58.

648 55. Mao, Z., and Davis, R.L. (2009). Eight different types of dopaminergic neurons
649 innervate the Drosophila mushroom body neuropil: anatomical and physiological
650 heterogeneity. Front Neural Circuits *3*, 5.

651 56. Chen, C.C., Wu, J.K., Lin, H.W., Pai, T.P., Fu, T.F., Wu, C.L., Tully, T., and Chiang, A.S.
652 (2012). Visualizing long-term memory formation in two neurons of the Drosophila
653 brain. Science *335*, 678-685.

654 57. Busch, S., Selcho, M., Ito, K., and Tanimoto, H. (2009). A map of octopaminergic
655 neurons in the Drosophila brain. J Comp Neurol *513*, 643-667.

656 58. Boto, T., Stahl, A., Zhang, X., Louis, T., and Tomchik, S.M. (2019). Independent
657 Contributions of Discrete Dopaminergic Circuits to Cellular Plasticity, Memory
658 Strength, and Valence in Drosophila. Cell Rep *27*, 2014-2021 e2012.

659 59. Warth Perez Arias, C.C., Frosch, P., Fiala, A., and Riemensperger, T.D. (2020).
660 Stochastic and Arbitrarily Generated Input Patterns to the Mushroom Bodies Can
661 Serve as Conditioned Stimuli in Drosophila. Front Physiol *11*, 53.

662 60. Hourcade, B., Muenz, T.S., Sandoz, J.C., Rossler, W., and Devaud, J.M. (2010). Long-
663 term memory leads to synaptic reorganization in the mushroom bodies: a memory
664 trace in the insect brain? J Neurosci *30*, 6461-6465.

665 61. Falibene, A., Roces, F., and Rossler, W. (2015). Long-term avoidance memory
666 formation is associated with a transient increase in mushroom body synaptic
667 complexes in leaf-cutting ants. Front Behav Neurosci *9*, 84.

668 62. Gupta, N., and Stopfer, M. (2014). A temporal channel for information in sparse
669 sensory coding. Curr Biol *24*, 2247-2256.

670 63. Haenicke, J., Yamagata, N., Zwaka, H., Nawrot, M., and Menzel, R. (2018). Neural
671 Correlates of Odor Learning in the Presynaptic Microglomerular Circuitry in the
672 Honeybee Mushroom Body Calyx. eNeuro *5*.

673 64. Gruntman, E., and Turner, G.C. (2013). Integration of the olfactory code across
674 dendritic claws of single mushroom body neurons. Nat Neurosci *16*, 1821-1829.

675 65. Delestro, F., Scheunemann, L., Pedrazzani, M., Tchenio, P., Preat, T., and Genovesio,
676 A. (2020). In vivo large-scale analysis of Drosophila neuronal calcium traces by
677 automated tracking of single somata. Scientific Reports *10*, 7153.

678 66. Saalfeld, S., Cardona, A., Hartenstein, V., and Tomancak, P. (2009). CATMAID:
679 collaborative annotation toolkit for massive amounts of image data. Bioinformatics
680 *25*, 1984-1986.

681 67. Prokop, A., and Meinertzhagen, I.A. (2006). Development and structure of synaptic
682 contacts in Drosophila. Semin Cell Dev Biol *17*, 20-30.

683 68. Tanaka, N.K., Tanimoto, H., and Ito, K. (2008). Neuronal assemblies of the Drosophila
684 mushroom body. J Comp Neurol *508*, 711-755.

685 69. Grabe, V., Strutz, A., Baschwitz, A., Hansson, B.S., and Sachse, S. (2015). Digital in vivo
686 3D atlas of the antennal lobe of Drosophila melanogaster. J Comp Neurol *523*, 530-
687 544.

688 70. Costa, M., Manton, J.D., Ostrovsky, A.D., Prohaska, S., and Jefferis, G.S. (2016).
689 NBLAST: Rapid, Sensitive Comparison of Neuronal Structure and Construction of
690 Neuron Family Databases. Neuron *91*, 293-311.

691 71. Cardona, A., Saalfeld, S., Schindelin, J., Arganda-Carreras, I., Preibisch, S., Longair, M.,
692 Tomancak, P., Hartenstein, V., and Douglas, R.J. (2012). TrakEM2 software for neural
693 circuit reconstruction. PLoS One *7*, e38011.

694 72. Cuntz, H., Forstner, F., Borst, A., and Hausser, M. (2011). The TREES toolbox--probing
695 the basis of axonal and dendritic branching. Neuroinformatics *9*, 91-96.

696 73. Schindelin, J., Arganda-Carreras, I., Frise, E., Kaynig, V., Longair, M., Pietzsch, T.,
697 Preibisch, S., Rueden, C., Saalfeld, S., Schmid, B., et al. (2012). Fiji: an open-source
698 platform for biological-image analysis. Nat Methods *9*, 676-682.

699 74. Louis, T., Stahl, A., Boto, T., and Tomchik, S.M. (2018). Cyclic AMP-dependent
700 plasticity underlies rapid changes in odor coding associated with reward learning.
701 Proc Natl Acad Sci U S A *115*, E448-E457.

702 75. Thevenaz, P., Ruttimann, U.E., and Unser, M. (1998). A pyramid approach to subpixel
703 registration based on intensity. IEEE Trans Image Process *7*, 27-41.

704